Journal of Quantitative Spectroscopy & Radiative Transfer 205 (2018) 241–252

Contents lists available at ScienceDirect

Journal of Quantitative Spectroscopy & Radiative Transfer

journal homepage: www.elsevier.com/locate/jqsrt

Far-field Lorenz–Mie scattering in an absorbing host medium: Theoretical formalism and FORTRAN program

Michael I. Mishchenko[a,*], Ping Yang[b]

[a] NASA Goddard Institute for Space Studies, 2880 Broadway, New York, NY 10025, USA
[b] Department of Atmospheric Sciences, Texas A&M University, College Station, TX 77843, USA

ARTICLE INFO

Article history:
Received 2 September 2017
Revised 20 October 2017
Accepted 20 October 2017

Keywords:
Far-field electromagnetic scattering
Absorbing host medium
Lorenz–Mie theory
Macroscopic Maxwell equations
Radiative transfer theory

ABSTRACT

In this paper we make practical use of the recently developed first-principles approach to electromagnetic scattering by particles immersed in an unbounded absorbing host medium. Specifically, we introduce an actual computational tool for the calculation of pertinent far-field optical observables in the context of the classical Lorenz–Mie theory. The paper summarizes the relevant theoretical formalism, explains various aspects of the corresponding numerical algorithm, specifies the input and output parameters of a FORTRAN program available at https://www.giss.nasa.gov/staff/mmishchenko/Lorenz-Mie.html, and tabulates benchmark results useful for testing purposes. This public-domain FORTRAN program enables one to solve the following two important problems: (i) simulate theoretically the reading of a remote well-collimated radiometer measuring electromagnetic scattering by an individual spherical particle or a small random group of spherical particles; and (ii) compute the single-scattering parameters that enter the vector radiative transfer equation derived directly from the Maxwell equations.

Published by Elsevier Ltd.

1. Introduction

Electromagnetic scattering by particles immersed in an unbounded absorbing host medium has been the subject of active yet somewhat controversial research [1–26]. Most of the controversy had stemmed from the enduring desire to preserve the conventional notions of the optical cross sections introduced in the context of electromagnetic scattering in a nonabsorbing host [27–29] as well as their traditional usage in the phenomenological radiative transfer equation [30–50]. The resolution of this controversy has come from (i) relying on the first-principles derivation of the entire theoretical formalism (including the radiative transfer theory) directly from the macroscopic Maxwell equations [21–23], and (ii) the realization that in the context of classical macroscopic electromagnetics, the introduction of an optical observable is only meaningful if it addresses one or both of the following two fundamental problems [51,52]:

- model theoretically the reading of a specific detector of electromagnetic radiation; and
- quantify the electromagnetic energy budget of a finite volume of space.

In the final analysis, it is the practical solution of these problems that demonstrates what theoretical notions are contrived and what optical observables emerge naturally and thereby serve as legitimate components of the scattering formalism.

The objective of this paper is to apply the main results of Refs. [21–23] to the development of a practical computational tool for the calculation of relevant far-field optical observables in the framework of the classical Lorenz–Mie theory of electromagnetic scattering by a homogeneous spherical particle embedded in an unbounded absorbing host medium [53]. We summarize all pertinent formulas, describe in detail the corresponding numerical algorithm, list the input and output parameters of the resulting public-domain FORTRAN program available at https://www.giss.nasa.gov/staff/mmishchenko/Lorenz-Mie.html, and tabulate benchmark numerical results useful for testing purposes. The quantities generated by this program can be used to solve the following two problems of actual practical significance:

1. quantify the reading of a remote polarization-sensitive well-collimated radiometer measuring electromagnetic scattering by an individual spherical particle or a small random group of spherical particles; and
2. compute the single-scattering parameters that enter the vector radiative transfer equation derived in Refs. [22,23] directly from the macroscopic Maxwell equations.

* Corresponding author.
E-mail address: michael.i.mishchenko@nasa.gov (M.I. Mishchenko).

https://doi.org/10.1016/j.jqsrt.2017.10.014
0022-4073/Published by Elsevier Ltd.

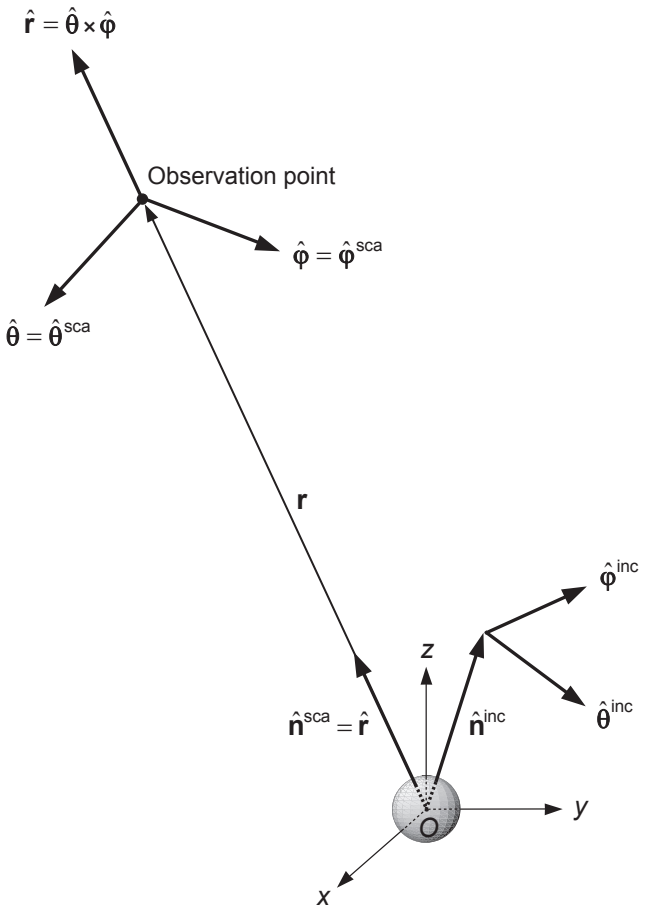

Fig. 1. Far-field electromagnetic scattering by a homogeneous spherical particle embedded in a homogeneous absorbing host medium.

Since this paper is intended, in particular, to serve as a detailed user guide to an actual computer program, we have tried to make it maximally self-contained. This explains the inclusion of more than 100 formulas, some of which are well known.

2. Far-field frequency-domain formalism

Consistent with Refs. [28,29,53], in this paper we assume the $\exp(-\mathrm{i}\omega t)$ time-harmonic dependence of all electromagnetic fields, where $\mathrm{i} = (-1)^{1/2}$, ω is the angular frequency, and t is time. Consider a fixed homogeneous spherical object embedded in an infinite, homogeneous, linear, isotropic, nonmagnetic, and, in general, absorbing host medium (see Section 9.25 of Ref. [53]). We assume that the object is made of an isotropic, linear, and nonmagnetic material. The central point O of the spherical object serves as the origin of the laboratory coordinate system and as the common origin of all position vectors $\mathbf{r}$ (Fig. 1). Let ε_1 and ε_2 be the complex-valued permittivities of the host medium and the scattering object, respectively, and μ_0 be the (real-valued) permeability of a vacuum. Then the wave numbers of the host and the object are given, respectively, by

$$k_1 = k_1' + \mathrm{i}k_1'' = \omega\sqrt{\varepsilon_1\mu_0} \tag{1}$$

and

$$k_2 = k_2' + \mathrm{i}k_2'' = \omega\sqrt{\varepsilon_2\mu_0}, \tag{2}$$

where $k'_1 > 0$, $k''_1 \geq 0$, $k'_2 > 0$, and $k''_2 \geq 0$. In practice, it is convenient to define the scattering problem in terms of the wavelength in a vacuum, λ, and the complex refractive indices of the host, m_1, and the object, m_2, given, respectively, by

$$m_1 = m_1' + \mathrm{i}m_1'' = \sqrt{\frac{\varepsilon_1}{\varepsilon_0}} \tag{3}$$

and

$$m_2 = m_2' + \mathrm{i}m_2'' = \sqrt{\frac{\varepsilon_2}{\varepsilon_0}}, \tag{4}$$

where ε_0 is the electric permittivity of a vacuum. Then

$$\omega = \frac{2\pi c}{\lambda}, \tag{5}$$

$$k_1 = \frac{2\pi m_1}{\lambda}, \tag{6}$$

and

$$k_2 = \frac{2\pi m_2}{\lambda}, \tag{7}$$

where

$$c = \frac{1}{\sqrt{\varepsilon_0\mu_0}} \tag{8}$$

is the speed of light in a vacuum.

To allow for an unambiguous definition of the Stokes parameters, let us further assume the incident field to be a *homogeneous* (or *uniform* [54]) plane electromagnetic wave propagating in the direction of the unit vector $\hat{\mathbf{n}}^{inc}$ and given by

$$\mathbf{E}^{inc}(\mathbf{r}) = \exp\left(\mathrm{i}k_1\hat{\mathbf{n}}^{inc}\cdot\mathbf{r}\right)\mathbf{E}_0^{inc}, \quad \mathbf{E}_0^{inc}\cdot\hat{\mathbf{n}}^{inc} = 0, \tag{9}$$

where $\mathbf{r}$ is the position vector of the observation point (Fig. 1). Note that $\mathbf{E}_0^{inc}$ is the electric field at the origin of the laboratory coordinate system. In the far zone of the object, the scattered field becomes an outgoing transverse spherical wave given by [21]

$$\begin{aligned}\mathbf{E}^{sca}(\mathbf{r}) &\underset{r\to\infty}{\to} \exp(-k''_1 r)\frac{\exp(\mathrm{i}k'_1 r)}{r}\mathbf{E}_1^{sca}(\hat{\mathbf{n}}^{sca}) \\ &= \exp(-k''_1 r)\frac{\exp(\mathrm{i}k'_1 r)}{r}\overleftrightarrow{A}(\hat{\mathbf{n}}^{sca},\hat{\mathbf{n}}^{inc})\cdot\mathbf{E}_0^{inc}.\end{aligned} \tag{10}$$

Here, $r = |\mathbf{r}|$ is the distance from the origin; $\hat{\mathbf{n}}^{sca} = \hat{\mathbf{r}} = \mathbf{r}/r$ is the unit vector in the scattering direction; and $\overleftrightarrow{A}(\hat{\mathbf{n}}^{sca},\hat{\mathbf{n}}^{inc})$ is the scattering dyadic such that

$$\hat{\mathbf{n}}^{sca}\cdot\overleftrightarrow{A}(\hat{\mathbf{n}}^{sca},\hat{\mathbf{n}}^{inc}) = \mathbf{0} \tag{11}$$

and

$$\overleftrightarrow{A}(\hat{\mathbf{n}}^{sca},\hat{\mathbf{n}}^{inc})\cdot\hat{\mathbf{n}}^{inc} = \mathbf{0}, \tag{12}$$

where $\mathbf{0}$ is a zero vector. Importantly, the angular and radial dependencies on the right-hand side of Eq. (10) are completely separated, so that the scattering dyadic is independent of r. The scattering dyadic has the dimension of length.

The total electric field at a far-field observation point is the sum of the incident and scattered fields:

$$\begin{aligned}\mathbf{E}(\mathbf{r}) &= \exp(\mathrm{i}k_1\hat{\mathbf{n}}^{inc}\cdot\mathbf{r})\mathbf{E}_0^{inc} + \exp(-k''_1 r) \\ &\quad\times\frac{\exp(\mathrm{i}k'_1 r)}{r}\overleftrightarrow{A}(\hat{\mathbf{n}}^{sca},\hat{\mathbf{n}}^{inc})\cdot\mathbf{E}_0^{inc}.\end{aligned} \tag{13}$$

It is straightforward to derive that the total far-field magnetic field is given by

$$\begin{aligned}\mathbf{H}(\mathbf{r}) &= \exp(\mathrm{i}k_1\hat{\mathbf{n}}^{inc}\cdot\mathbf{r})\frac{k_1}{\omega\mu_0}\hat{\mathbf{n}}^{inc}\times\mathbf{E}_0^{inc} + \exp(-k''_1 r) \\ &\quad\times\frac{\exp(\mathrm{i}k'_1 r)}{r}\frac{k_1}{\omega\mu_0}\hat{\mathbf{n}}^{sca}\times[\overleftrightarrow{A}(\hat{\mathbf{n}}^{sca},\hat{\mathbf{n}}^{inc})\cdot\mathbf{E}_0^{inc}].\end{aligned} \tag{14}$$

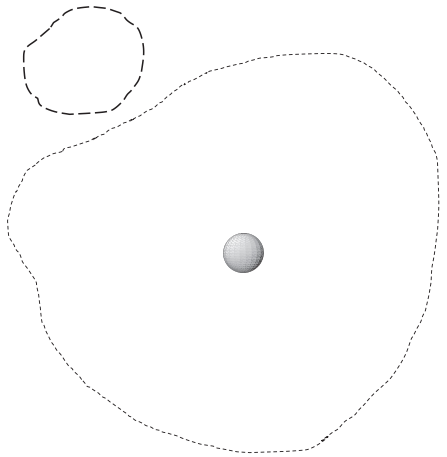

Fig. 2. Examples of finite far-field volumes.

The transversality of the incident and scattered waves allows us to rewrite Eq. (10) in terms of the θ- and φ-components of the corresponding electric field vectors (Fig. 1):

$$\begin{bmatrix} E_{1\theta}^{\rm sca}(\hat{\mathbf{n}}^{\rm sca}) \\ E_{1\varphi}^{\rm sca}(\hat{\mathbf{n}}^{\rm sca}) \end{bmatrix} = \mathbf{S}(\hat{\mathbf{n}}^{\rm sca}, \hat{\mathbf{n}}^{\rm inc}) \begin{bmatrix} E_{0\theta}^{\rm inc} \\ E_{0\varphi}^{\rm inc} \end{bmatrix}. \tag{15}$$

The elements of the amplitude scattering matrix $\mathbf{S}$ have the dimension of length and are expressed in terms of the scattering dyadic as follows:

$$S_{11} = \hat{\boldsymbol{\theta}}^{\rm sca} \cdot \overleftrightarrow{A} \cdot \hat{\boldsymbol{\theta}}^{\rm inc}, \tag{16}$$

$$S_{12} = \hat{\boldsymbol{\theta}}^{\rm sca} \cdot \overleftrightarrow{A} \cdot \hat{\boldsymbol{\varphi}}^{\rm inc}, \tag{17}$$

$$S_{21} = \hat{\boldsymbol{\varphi}}^{\rm sca} \cdot \overleftrightarrow{A} \cdot \hat{\boldsymbol{\theta}}^{\rm inc}, \tag{18}$$

$$S_{22} = \hat{\boldsymbol{\varphi}}^{\rm sca} \cdot \overleftrightarrow{A} \cdot \hat{\boldsymbol{\varphi}}^{\rm inc}, \tag{19}$$

where $\hat{\boldsymbol{\theta}}$ and $\hat{\boldsymbol{\varphi}}$ are the corresponding spherical-coordinate unit vectors.

3. Energy budget of a finite far-field volume element

Let us consider the energy budget of a finite volume V such that all points of its closed surface S reside in the far zone of the spherical particle. The particle can be either inside V, as illustrated by the short-dashed contour in Fig. 2, or outside V, as shown by the long-dashed contour. The time-averaged rate at which the electromagnetic energy crosses S is given by the Stokes theorem [53]:

$$W = -\frac{1}{2}{\rm Re}\int_S {\rm d}^2\mathbf{r}\,[\mathbf{E}(\mathbf{r}) \times \mathbf{H}^*(\mathbf{r})] \cdot \hat{\mathbf{n}}(\mathbf{r}), \tag{20}$$

where $\hat{\mathbf{n}}(\mathbf{r})$ is a unit vector in the direction of the local outward normal to S, $\mathbf{E}(\mathbf{r})$ and $\mathbf{H}(\mathbf{r})$ are given by Eqs. (13) and (14), respectively, and the asterisk denotes a complex-conjugate value. Thus Eqs. (13), (14), and (20) define the time-averaged electromagnetic energy budget of a finite volume bounded by a far-field surface.

In the case of a nonabsorbing host medium, W would be independent of S. For example, it would vanish in the case of S represented by the long-dashed contour in Fig. 2, while in the case of the surface depicted by the short-dashed contour it would be the same as for a sufficiently large spherical volume centered at the particle.

In the case of an absorbing host medium, W never vanishes and is an explicit function of S. As a consequence, it is impossible to derive a general simple analytical expression for S and introduce such conventional far-field optical characteristics of the particle as its scattering and absorption cross sections.

4. Far-field optical observables describing measurements with a well-collimated polarization-sensitive radiometer

Let us now assume that $\hat{\mathbf{n}}^{\rm inc} = \hat{\mathbf{z}}$ and $\varphi^{\rm sca} = \varphi^{\rm inc}$, where $\hat{\mathbf{z}}$ is the unit vector along the positive direction of the z axis. In this case

$$\mathbf{S}(\hat{\mathbf{n}}^{\rm sca}, \hat{\mathbf{n}}^{\rm inc}) = \begin{bmatrix} S_{11}(\Theta) & 0 \\ 0 & S_{22}(\Theta) \end{bmatrix}, \tag{21}$$

where $\Theta = \theta^{\rm sca}$ is the angle between the incidence and scattering directions, i.e., the scattering angle.

The Stokes parameters of the incident plane wave and the scattered spherical wave are given, respectively, by [21]

$$\mathbf{I}^{\rm inc} = \begin{bmatrix} I^{\rm inc} \\ Q^{\rm inc} \\ U^{\rm inc} \\ V^{\rm inc} \end{bmatrix} = \frac{k'_1}{2\omega\mu_0} \begin{bmatrix} E_{0\theta}^{\rm inc}(E_{0\theta}^{\rm inc})^* + E_{0\varphi}^{\rm inc}(E_{0\varphi}^{\rm inc})^* \\ E_{0\theta}^{\rm inc}(E_{0\theta}^{\rm inc})^* - E_{0\varphi}^{\rm inc}(E_{0\varphi}^{\rm inc})^* \\ -E_{0\theta}^{\rm inc}(E_{0\varphi}^{\rm inc})^* - E_{0\varphi}^{\rm inc}(E_{0\theta}^{\rm inc})^* \\ {\rm i}[E_{0\varphi}^{\rm inc}(E_{0\theta}^{\rm inc})^* - E_{0\theta}^{\rm inc}(E_{0\varphi}^{\rm inc})^*] \end{bmatrix} \tag{22}$$

and

$$\mathbf{I}^{\rm sca}(r,\Theta) = \begin{bmatrix} I^{\rm sca}(r,\Theta) \\ Q^{\rm sca}(r,\Theta) \\ U^{\rm sca}(r,\Theta) \\ V^{\rm sca}(r,\Theta) \end{bmatrix} = \frac{\exp(-2k''_1 r)}{r^2}\frac{k'_1}{2\omega\mu_0} \begin{bmatrix} E_{1\theta}^{\rm sca}(E_{1\theta}^{\rm sca})^* + E_{1\varphi}^{\rm sca}(E_{1\varphi}^{\rm sca})^* \\ E_{1\theta}^{\rm sca}(E_{1\theta}^{\rm sca})^* - E_{1\varphi}^{\rm sca}(E_{1\varphi}^{\rm sca})^* \\ -E_{1\theta}^{\rm sca}(E_{1\varphi}^{\rm sca})^* - E_{1\varphi}^{\rm sca}(E_{1\theta}^{\rm sca})^* \\ {\rm i}[E_{1\varphi}^{\rm sca}(E_{1\theta}^{\rm sca})^* - E_{1\theta}^{\rm sca}(E_{1\varphi}^{\rm sca})^*] \end{bmatrix}. \tag{23}$$

Note that both sets of the Stokes parameters are defined with respect to the common scattering plane, i.e., the plane through the incidence and scattering directions. Then

$$\mathbf{I}^{\rm sca}(r,\Theta) = \frac{\exp(-2k''_1 r)}{r^2}\mathbf{F}(\Theta)\mathbf{I}^{\rm inc}, \tag{24}$$

where

$$\mathbf{F}(\Theta) = \begin{bmatrix} F_{11}(\Theta) & F_{12}(\Theta) & 0 & 0 \\ F_{21}(\Theta) & F_{22}(\Theta) & 0 & 0 \\ 0 & 0 & F_{33}(\Theta) & F_{34}(\Theta) \\ 0 & 0 & F_{43}(\Theta) & F_{44}(\Theta) \end{bmatrix} \tag{25}$$

is the scattering matrix with non-zero elements given by

$$F_{11}(\Theta) = F_{22}(\Theta) = \frac{1}{2}[|S_{11}(\Theta)|^2 + |S_{22}(\Theta)|^2], \tag{26}$$

$$F_{33}(\Theta) = F_{44}(\Theta) = {\rm Re}[S_{11}(\Theta)S_{22}^*(\Theta)], \tag{27}$$

$$F_{12}(\Theta) = F_{21}(\Theta) = \frac{1}{2}[|S_{11}(\Theta)|^2 - |S_{22}(\Theta)|^2], \tag{28}$$

and

$$F_{34}(\Theta) = -F_{43}(\Theta) = {\rm Im}[S_{11}(\Theta)S_{22}^*(\Theta)]. \tag{29}$$

Note that "Re" stands for "real part of" and "Im" stands for "imaginary part of". Again, the radial and angular dependencies on the right-hand side of Eq. (24) are separated. The scattering matrix has the dimension of area.

Let us now assume that a polarization-sensitive well-collimated radiometer [51,55] is located in the far zone of the spherical particle and is centered at the origin O such that its optical axis is

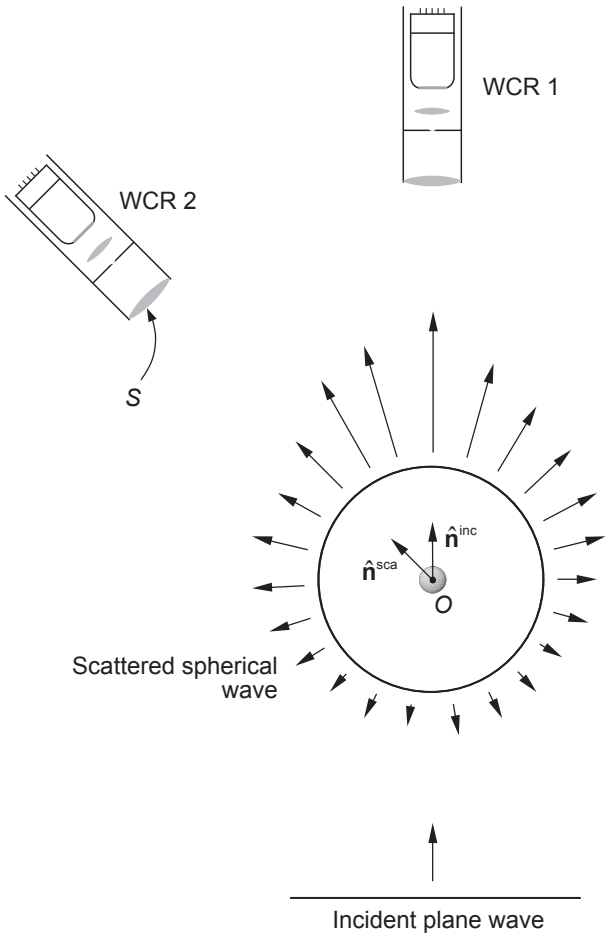

Fig. 3. Far-field measurements with well-collimated radiometers.

aligned along the unit vector $\hat{\mathbf{n}}^{\rm sca} \neq \hat{\mathbf{z}}$ (WCR 2 in Fig. 3). Then the polarized reading of this detector is given by [21]

$$\textbf{Signal 2} = S\mathbf{I}^{\rm sca}(r,\Theta) = \frac{\exp(-2k''_1 r)}{r^2} S\mathbf{F}(\Theta)\mathbf{I}^{\rm inc}, \tag{30}$$

where S is the area of the objective lens of the detector. If, however, $\hat{\mathbf{n}}^{\rm sca} = \hat{\mathbf{z}}$ (WCR 1 in Fig. 3) then the polarized signal recorded by the detector is [21]

$$\textbf{Signal 1} = \exp(-2k''_1 r) S\mathbf{I}^{\rm inc} + \frac{\exp(-2k''_1 r)}{r^2} S\mathbf{F}(0)\mathbf{I}^{\rm inc} - \exp(-2k''_1 r) C_{\rm ext}\mathbf{I}^{\rm inc}, \tag{31}$$

where the extinction cross section is given by

$$C_{\rm ext} = \frac{2\pi}{k'_1}{\rm Im}[S_{11}(0) + S_{22}(0)] = \frac{4\pi}{k'_1}{\rm Im}S_{11}(0) \tag{32}$$

and has the dimension of area.

Thus the readings of the two far-field well-collimated polarization-sensitive radiometers can be quantized in terms of the distance-independent scattering matrix and extinction cross section of the particle.

5. Amplitude scattering matrix

The non-zero elements of the amplitude scattering matrix entering Eqs. (26)–(29) and (32) are given by [28,29,53]

$$S_{11}(\Theta) = \frac{\rm i}{k_1}\sum_{n=1}^{\infty}\frac{2n+1}{n(n+1)}[a_n\tau_n(\Theta) + b_n\pi_n(\Theta)] \tag{33}$$

and

$$S_{22}(\Theta) = \frac{\rm i}{k_1}\sum_{n=1}^{\infty}\frac{2n+1}{n(n+1)}[a_n\pi_n(\Theta) + b_n\tau_n(\Theta)], \tag{34}$$

where the angular functions are expressed in terms of the associated Legendre functions $P_n^m(\cos\Theta)$ or Wigner d-functions $d_{mm'}^n(\Theta)$ (see Appendix F of Ref. [56]) according to

$$\pi_n(\Theta) = -\frac{P_n^1(\cos\Theta)}{\sin\Theta} = \sqrt{n(n+1)}\frac{d_{01}^n(\Theta)}{\sin\Theta} \tag{35}$$

and

$$\tau_n(\Theta) = -\frac{{\rm d}P_n^1(\cos\Theta)}{{\rm d}\Theta} = \sqrt{n(n+1)}\frac{{\rm d}d_{01}^n(\Theta)}{{\rm d}\Theta}, \tag{36}$$

while the dimensionless so-called Lorenz–Mie coefficients a_n and b_n are given by [28,53]

$$a_n = \frac{m^2 j_n(mx_1)[x_1 j_n(x_1)]' - j_n(x_1)[mx_1 j_n(mx_1)]'}{m^2 j_n(mx_1)[x_1 h_n^{(1)}(x_1)]' - h_n^{(1)}(x_1)[mx_1 j_n(mx_1)]'} \tag{37}$$

and

$$b_n = \frac{j_n(mx_1)[x_1 j_n(x_1)]' - j_n(x_1)[mx_1 j_n(mx_1)]'}{j_n(mx_1)[x_1 h_n^{(1)}(x_1)]' - h_n^{(1)}(x_1)[mx_1 j_n(mx_1)]'}. \tag{38}$$

In the last two formulas,

$$m = \frac{m_2}{m_1} \tag{39}$$

is the refractive index of the spherical particle relative to that of the host medium,

$$x_1 = k_1 R \tag{40}$$

is the (generally complex-valued) size parameter of the particle,

$$j_n(z) = z^n\left(-\frac{1}{z}\frac{\rm d}{{\rm d}z}\right)^n\left(\frac{\sin z}{z}\right) \tag{41}$$

are spherical Bessel functions of the first kind, and

$$h_n^{(1)}(z) = j_n(z) + {\rm i}y_n(z) \tag{42}$$

are Hankel functions of the first kind, where

$$y_n(z) = -z^n\left(-\frac{1}{z}\frac{\rm d}{{\rm d}z}\right)^n\left(\frac{\cos z}{z}\right) \tag{43}$$

are spherical Bessel functions of the second kind.

The well-known property

$$\pi_n(0) = \tau_n(0) = \frac{1}{2}n(n+1) \tag{44}$$

implies that

$$C_{\rm ext} = \frac{2\pi}{k'_1}{\rm Re}\sum_{n=1}^{\infty}\frac{1}{k_1}(2n+1)(a_n + b_n). \tag{45}$$

This formula corrects Eq. (11) of Bohren and Gilra [3]. If the host medium is nonabsorbing then $k_1 = k'_1$, and Eq. (45) reduces to the standard result of the conventional Lorenz–Mie theory [27–29].

6. Derivative scattering characteristics

It is convenient to define the so-called effective scattering cross section according to

$$C_{\rm sca}^{\rm eff} = 2\pi\int_0^{\pi}{\rm d}\Theta\sin\Theta\, F_{11}(\Theta) \tag{46}$$

and the so-called normalized scattering matrix according to

$$\tilde{\mathbf{F}}(\Theta) = \frac{4\pi}{C_{\rm sca}^{\rm eff}}\mathbf{F}(\Theta). \tag{47}$$

$C_{\rm sca}^{\rm eff}$ has the dimension of area, while $\tilde{\mathbf{F}}(\Theta)$ is dimensionless. It is easily verified that the (1,1) element of the normalized scattering matrix, often referred to as the phase function, is normalized to unity according to

$$\frac{1}{2}\int_0^\pi \mathrm{d}\Theta \sin\Theta\, \tilde{F}_{11}(\Theta) = 1. \tag{48}$$

The integral in Eq. (46) can be evaluated using Eqs. (26), (33), and (34) along with the well-known orthogonality relations

$$\int_0^\pi \mathrm{d}\Theta \sin\Theta\, [\pi_n(\Theta)\pi_{n'}(\Theta) + \tau_n(\Theta)\tau_{n'}(\Theta)] = \delta_{nn'}\frac{2n^2(n+1)^2}{2n+1} \tag{49}$$

and

$$\int_0^\pi \mathrm{d}\Theta \sin\Theta\, [\pi_n(\Theta)\tau_{n'}(\Theta) + \pi_{n'}(\Theta)\tau_n(\Theta)] = 0, \tag{50}$$

where $\delta_{nn'}$ is the Kronecker delta. The result is

$$C_{\rm sca}^{\rm eff} = \frac{2\pi}{|k_1|^2}\sum_{n=1}^{\infty}(2n+1)(|a_n|^2 + |b_n|^2). \tag{51}$$

If $k''_1 = 0$ then Eq. (51) reduces to the well-known result of the Lorenz–Mie theory derived for the case of a nonabsorbing host medium [27–29]. It is imperative to remember, however, that $C_{\rm sca}^{\rm eff}$ cannot be interpreted in the same way as the conventional scattering cross section.

7. Random spherical particle

Let us now consider what can be called a random spherical particle by allowing the position and radius of the spherical scattering object in Figs. 1 and 3 to fluctuate in time (cf. Chapter 6 of Ref. [56]). We assume however that the particle is confined to an imaginary residence volume which is centered at O and has dimensions much smaller than the distance r from O to the observation point. Note that although the distance from either radiometer shown in Fig. 3 to O is large enough for the radiometer to be in the far zone of a particle centered at O, it may be insufficient for the radiometer to be in the far zone of the entire residence volume. Owing to the random fluctuations of the particle radius R and position, the readings of the two radiometers defined in Section 4 are random functions of time. Let us however assume that (i) both readings are ergodic random processes (this allows us to replace time averaging with ensemble averaging), and (ii) the random variations of the particle radius are restricted according to $R \in [R_{\min}, R_{\max}]$ and described by an appropriate normalized probability density function $n(R)$ such that $n(R)\mathrm{d}R$ is the fraction of time during which the particle radius has a value between R and $R + \mathrm{d}R$, so that

$$\int_{R_{\min}}^{R_{\max}} \mathrm{d}R\, n(R) = 1. \tag{52}$$

It can then be shown that the time averages of the two readings are given by

$$\langle \textbf{Signal 1}\rangle_t = \exp(-2k''_1 r)S\mathbf{I}^{\rm inc} + \frac{\exp(-2k''_1 r)}{r^2}S\langle \mathbf{F}(0)\rangle_R \mathbf{I}^{\rm inc} - \exp(-2k''_1 r)\langle C_{\rm ext}\rangle_R \mathbf{I}^{\rm inc}, \tag{53}$$

$$\langle \textbf{Signal 2}\rangle_t = \frac{\exp(-2k''_1 r)}{r^2}S\langle \mathbf{F}(\Theta)\rangle_R \mathbf{I}^{\rm inc}, \tag{54}$$

where

$$\langle \mathbf{F}(\Theta)\rangle_R = \int_{R_{\min}}^{R_{\max}} \mathrm{d}R\, n(R)\mathbf{F}(\Theta, R) \tag{55}$$

and

$$\langle C_{\rm ext}\rangle_R = \int_{R_{\min}}^{R_{\max}} \mathrm{d}R\, n(R) C_{\rm ext}(R), \tag{56}$$

$\mathbf{F}(\Theta, R)$ being the scattering matrix and $C_{\rm ext}(R)$ being the extinction cross section of a particle having a radius R.

The resulting normalized scattering matrix is calculated according to

$$\tilde{\mathbf{F}}(\Theta) = \frac{4\pi}{\langle C_{\rm sca}^{\rm eff}\rangle_R}\langle \mathbf{F}(\Theta)\rangle_R = \begin{bmatrix} a_1(\Theta) & b_1(\Theta) & 0 & 0 \\ b_1(\Theta) & a_2(\Theta) & 0 & 0 \\ 0 & 0 & a_3(\Theta) & b_2(\Theta) \\ 0 & 0 & -b_2(\Theta) & a_4(\Theta) \end{bmatrix}. \tag{57}$$

In this formula,

$$\langle C_{\rm sca}^{\rm eff}\rangle_R = \int_{R_{\min}}^{R_{\max}} \mathrm{d}R\, n(R) C_{\rm sca}^{\rm eff}(R), \tag{58}$$

where the radius-specific effective scattering cross section $C_{\rm sca}^{\rm eff}(R)$ is given by Eq. (51), $a_2(\Theta) \equiv a_1(\Theta)$, $a_4(\Theta) \equiv a_3(\Theta)$, and $a_1(\Theta)$ is normalized according to Eq. (48).

8. Sparse random group of spherical particles

Let us now consider a small sparse group of N random particles (cf. Chapter 14 of Ref. [51]). Again, we assume that (i) these particles are confined to an imaginary residence volume which is centered at O and has dimensions much smaller than the distance from O to the observation point, and (ii) the reading of either well-collimated radiometer shown in Fig. 3 is ergodic. Then we have instead of Eqs. (30) and (31):

$$\langle \textbf{Signal 1}\rangle_t = \exp(-2k''_1 r)S\mathbf{I}^{\rm inc} + \frac{\exp(-2k''_1 r)}{r^2}SN\langle \mathbf{F}(0)\rangle_R \mathbf{I}^{\rm inc} - \exp(-2k''_1 r)N\langle C_{\rm ext}\rangle_R \mathbf{I}^{\rm inc} \tag{59}$$

and

$$\langle \textbf{Signal 2}\rangle_t = N\frac{\exp(-2k''_1 r)}{r^2}S\langle \mathbf{F}(\Theta)\rangle_R \mathbf{I}^{\rm inc}, \tag{60}$$

where the ensemble averages of the scattering matrix and extinction cross section per particle are given by Eqs. (55) and (56) in which the probability density function $n(R)$ now characterizes the entire N-particle ensemble. In other words, $n(R)\mathrm{d}R$ is the fraction of time during which the radius of any particle in the ensemble has a value between R and $R + \mathrm{d}R$. Eqs. (57) and (58) remain unchanged.

9. Radiative transfer theory

The object of study in the first-principles radiative transfer theory is a very large random ensemble of widely separated particles forming what is traditionally referred to as a sparse discrete random medium or a turbid medium [51,52,56,57]. By solving the so-called vector radiative transfer equation, one can solve both problems formulated in the Introduction, i.e., quantify the electromagnetic energy budget of a finite volume of discrete random medium and simulate theoretically the (polarized) reading of a well-collimated radiometer located inside or outside the multiparticle group (see, in particular, Sections 19.10–19.12 of Ref. [51]). It was shown in Ref. [23] that in the case of a turbid medium composed of spherically symmetric particles, the radiative transfer equation reads

$$\hat{\mathbf{q}}\cdot\nabla\tilde{\mathbf{I}}(\mathbf{r}, \hat{\mathbf{q}}) = -(2k''_1 + n_0\langle C_{\rm ext}\rangle_R)\tilde{\mathbf{I}}(\mathbf{r}, \hat{\mathbf{q}}) + \frac{n_0\langle C_{\rm sca}^{\rm eff}\rangle_R}{4\pi}\int_{4\pi}\mathrm{d}\hat{\mathbf{q}}'\tilde{\mathbf{Z}}(\hat{\mathbf{q}}, \hat{\mathbf{q}}')\tilde{\mathbf{I}}(\mathbf{r}, \hat{\mathbf{q}}'), \tag{61}$$

where

- $\mathbf{r}$ is position vector of the observation point relative to the laboratory coordinate system;
- the bold characters with carets denote unit vectors in the corresponding "propagation" directions;
- $\tilde{\mathbf{I}}(\mathbf{r}, \hat{\mathbf{q}})$ is the four-element so-called specific intensity column vector at the observation point $\mathbf{r}$ for the propagation direction $\hat{\mathbf{q}}$;
- n_0 is the number of particles per unit volume of discrete random medium; and
- $\tilde{\mathbf{Z}}(\hat{\mathbf{q}}, \hat{\mathbf{q}}')$ is the 4×4 so-called normalized phase matrix obtained from $\tilde{\mathbf{F}}(\Theta)$ by means of the standard pre- and post-multiplication of $\tilde{\mathbf{F}}(\Theta)$ by 4×4 rotation matrices, the result being that $\tilde{\mathbf{Z}}(\hat{\mathbf{q}}, \hat{\mathbf{q}}')$ describes the single-scattering relationship between the initial and final specific intensity column vectors defined relative to their respective meridional planes rather than relative to the common scattering plane (see, e.g., Section 11.3 in Ref. [56]).

It is thus clear that if $\langle C_{\rm ext}\rangle_R$, $\langle C_{\rm sca}^{\rm eff}\rangle_R$, and $\tilde{\mathbf{F}}(\Theta)$ are known then Eq. (61) becomes fully defined and can be solved numerically.

10. Expansion in Wigner *d*-functions

A numerically convenient analytical representation of the elements of the normalized scattering matrix (57) [41,58,59] is the expansion in so-called generalized spherical functions $P_{pq}^s(\cos\Theta)$ or, equivalently, in Wigner d-functions $d_{pq}^s(\Theta) = \mathrm{i}^{q-p} P_{pq}^s(\cos\Theta)$ (see Appendix F of Ref. [56]):

$$a_1(\Theta) = \sum_{s=0}^{s_{\max}} \alpha_1^s P_{00}^s(\cos\Theta) = \sum_{s=0}^{s_{\max}} \alpha_1^s d_{00}^s(\Theta), \tag{62}$$

$$\begin{aligned} a_2(\Theta) + a_3(\Theta) &= \sum_{s=0}^{s_{\max}} (\alpha_2^s + \alpha_3^s) P_{22}^s(\cos\Theta) \\ &= \sum_{s=0}^{s_{\max}} (\alpha_2^s + \alpha_3^s) d_{22}^s(\Theta), \end{aligned} \tag{63}$$

$$\begin{aligned} a_2(\Theta) - a_3(\Theta) &= \sum_{s=0}^{s_{\max}} (\alpha_2^s - \alpha_3^s) P_{2,-2}^s(\cos\Theta) \\ &= \sum_{s=0}^{s_{\max}} (\alpha_2^s - \alpha_3^s) d_{2,-2}^s(\Theta), \end{aligned} \tag{64}$$

$$a_4(\Theta) = \sum_{s=0}^{s_{\max}} \alpha_4^s P_{00}^s(\cos\Theta) = \sum_{s=0}^{s_{\max}} \alpha_4^s d_{00}^s(\Theta), \tag{65}$$

$$b_1(\Theta) = \sum_{s=0}^{s_{\max}} \beta_1^s P_{02}^s(\cos\Theta) = -\sum_{s=0}^{s_{\max}} \beta_1^s d_{02}^s(\Theta), \tag{66}$$

$$b_2(\Theta) = \sum_{s=0}^{s_{\max}} \beta_2^s P_{02}^s(\cos\Theta) = -\sum_{s=0}^{s_{\max}} \beta_2^s d_{02}^s(\Theta), \tag{67}$$

where the upper summation limit $s_{\max}$ depends on the requisite numerical accuracy of these series. Indeed, the knowledge of the finite set of expansion coefficients allows one to compute the normalized scattering matrix for an arbitrary set of scattering angles with a minimal expense of computer time. Furthermore, these expansion coefficients can expedite the computation of the phase matrix entering the vector radiative transfer equation.

The orthogonality property of the generalized spherical functions and the Wigner d-functions (see Appendix F of Ref. [56]) implies that

$$\alpha_1^s = \left(s + \frac{1}{2}\right) \int_0^\pi \mathrm{d}\Theta \sin\Theta \, a_1(\Theta) d_{00}^s(\Theta), \tag{68}$$

$$\alpha_2^s + \alpha_3^s = \left(s + \frac{1}{2}\right) \int_0^\pi \mathrm{d}\Theta \sin\Theta [a_2(\Theta) + a_3(\Theta)] d_{22}^s(\Theta), \tag{69}$$

$$\alpha_2^s - \alpha_3^s = \left(s + \frac{1}{2}\right) \int_0^\pi \mathrm{d}\Theta \sin\Theta [a_2(\Theta) - a_3(\Theta)] d_{2,-2}^s(\Theta), \tag{70}$$

$$\alpha_4^s = \left(s + \frac{1}{2}\right) \int_0^\pi \mathrm{d}\Theta \sin\Theta a_4(\Theta) d_{00}^s(\Theta), \tag{71}$$

$$\beta_1^s = -\left(s + \frac{1}{2}\right) \int_0^\pi \mathrm{d}\Theta \sin\Theta b_1(\Theta) d_{02}^s(\Theta), \tag{72}$$

$$\beta_2^s = -\left(s + \frac{1}{2}\right) \int_0^\pi \mathrm{d}\Theta \sin\Theta b_2(\Theta) d_{02}^s(\Theta). \tag{73}$$

Note that Eq. (62) is the standard expansion of the phase function in terms of Legendre polynomials $P_s(\cos\Theta)$. The normalization (48) implies that

$$\alpha_1^0 \equiv 1. \tag{74}$$

11. Numerical procedure

In accordance with the previous discussion, the main output generated by a far-field computer program based on the Lorenz–Mie theory can consist of the ensemble-averaged extinction cross section given by Eqs. (45) and (56); the expansion coefficients given by Eqs. (68)–(73); and the ensemble-averaged effective scattering cross section given by Eqs. (51) and (58). The normalized scattering matrix and the ensemble-averaged scattering matrix can then be computed for any set of scattering angles using Eqs. (62)–(67) and (57).

The sequence of major steps required to generate this output is as follows:

1. Compute the amplitude scattering matrix (21) for an appropriate discrete set of particle radii R and scattering angles Θ.
2. Compute the size-averaged scattering matrix (55), extinction cross section (56), and effective scattering cross section (58).
3. Compute the normalized scattering matrix (57) and the expansion coefficients (68)–(73).

Below we briefly describe the specific numerical implementation of these steps in our computer program.

11.1. Calculation of the amplitude scattering matrix for a fixed spherical particle

In practical computer calculations, the infinite series of Eqs. (33) and (34) are truncated to a finite size $n_{\max}$ that depends on the particle size parameter x_1. A simple empirical criterion for choosing $n_{\max}$ adopted in our code is

$$n_{\max}(x_1) = |x_1| + 4.05|x_1|^{1/3} + 8. \tag{75}$$

This criterion is somewhat more conservative than that proposed by Wiscombe [60] and as such typically yields results that are accurate to a few more decimals.

The spherical Bessel functions of the first kind, $j_n(z)$ (where z is equal to x_1 or mx_1 and is, in general, complex), obey the recurrence relation [61]

$$j_{n+1}(z) = \frac{2n+1}{z} j_n(z) - j_{n-1}(z). \tag{76}$$

Since the upward recurrence relation for $j_n(z)$ is unstable, we define

$$r_n(z) = \frac{j_n(z)}{j_{n-1}(z)}, \tag{77}$$

which leads to the stable downward recurrence relation

$$r_n(z) = \left[\frac{2n+1}{z} - r_{n+1}(z)\right]^{-1}. \tag{78}$$

For $n \gg |z|$, we have

$$r_n(z) \underset{n\gg|z|}{\approx} \frac{z}{2n+1}. \tag{79}$$

If $n_{\max}$ is the largest n-value, we start the downward recursion of Eq. (78) at $n = n_{\max} + n'$, where n' is chosen such that by the time n has been reduced to $n_{\max}$, the *relative* error in $r_{n_{\max}}(z)$ caused by using the approximate asymptotic formula (79) becomes negligibly small. We then compute $j_n(z)$ using the straightforward upward recursion

$$j_n(z) = r_n(z) j_{n-1}(z), \tag{80}$$

starting at

$$j_1(z) = r_1(z) j_0(z) \quad \text{with} \quad j_0(z) = \frac{\sin z}{z}. \tag{81}$$

We also use the recurrence relation [61]

$$\frac{\mathrm{d}}{\mathrm{d}z}[z j_n(z)] = z j_{n-1}(z) - n j_n(z). \tag{82}$$

To compute the Hankel functions of the first kind and their derivatives, we first find the spherical Bessel functions of the first kind, as described above, and then compute the spherical Bessel functions of the second kind using the numerically stable upward recursion

$$y_{n+1}(z) = \frac{2n+1}{z} y_n(z) - y_{n-1}(z) \tag{83}$$

combined with the initial values

$$y_0(z) = -\frac{\cos z}{z} \quad \text{and} \quad y_1(z) = -\frac{\cos z}{z^2} - \frac{\sin z}{z}. \tag{84}$$

Finally, we use the recurrence formula [61]

$$\frac{\mathrm{d}}{\mathrm{d}z}[z y_n(z)] = z y_{n-1}(z) - n y_n(z). \tag{85}$$

The angular functions are computed using the recurrence relations [60]

$$\pi_{n+1}(\Theta) = s + \frac{n+1}{n} t \tag{86}$$

and

$$\tau_n(\Theta) = nt - \pi_{n-1}(\Theta), \tag{87}$$

supplemented by the initial values

$$\pi_0(\Theta) = 0 \quad \text{and} \quad \pi_1(\Theta) = 1, \tag{88}$$

where $s = \cos\Theta \pi_n(\Theta)$ and $t = s - \pi_{n-1}(\Theta)$.

11.2. Calculation of the ensemble-averaged quantities

The computation of the polydisperse extinction and effective scattering cross sections and the scattering matrix per particle is straightforward:

$$\langle C_{\text{ext}} \rangle_R \approx \sum_{i=1}^{N_R} u_i n(R_i) C_{\text{ext}}(R_i), \tag{89}$$

$$\langle C_{\text{sca}}^{\text{eff}} \rangle_R \approx \sum_{i=1}^{N_R} u_i n(R_i) C_{\text{sca}}^{\text{eff}}(R_i), \tag{90}$$

$$\langle \mathbf{F}(\Theta) \rangle_R \approx \sum_{i=1}^{N_R} u_i n(R_i) \mathbf{F}(\Theta, R_i), \tag{91}$$

where R_i and u_i are the division points and weights, respectively, of a quadrature formula on the interval $[R_{\min}, R_{\max}]$. It may not be easy to give an *a priori* estimate of the number N_R of quadrature division points in Eqs. (89)–(91). In practice, this number needs to be increased until all relevant scattering characteristics converge within a given accuracy. The actual numerical integration over the size distribution in our computer program is performed by subdividing the whole interval $[R_{\min}, R_{\max}]$ of particle radii into a number of equal subintervals and applying a Gaussian quadrature formula with a fixed number of division points to each such subinterval.

11.3. Calculation of the normalized scattering matrix and expansion coefficients

The normalized scattering matrix is given by Eq. (57). Following de Rooij and van der Stap [58], the resulting expansion coefficients are computed by evaluating numerically the angular integrals in Eqs. (68)–(73). Specifically,

$$\alpha_1^s \approx \left(s + \frac{1}{2}\right) \sum_{j=1}^{N_\Theta} w_j a_1(\arccos\mu_j) d_{00}^s(\arccos\mu_j), \tag{92}$$

$$\alpha_2^s + \alpha_3^s \approx \left(s + \frac{1}{2}\right) \sum_{j=1}^{N_\Theta} w_j [a_2(\arccos\mu_j) + a_3(\arccos\mu_j)] d_{22}^s(\arccos\mu_j), \tag{93}$$

$$\alpha_2^s - \alpha_3^s \approx \left(s + \frac{1}{2}\right) \sum_{j=1}^{N_\Theta} w_j [a_2(\arccos\mu_j) - a_3(\arccos\mu_j)] d_{2,-2}^s(\arccos\mu_j), \tag{94}$$

$$\alpha_4^s \approx \left(s + \frac{1}{2}\right) \sum_{j=1}^{N_\Theta} w_j a_4(\arccos\mu_j) d_{00}^s(\arccos\mu_j), \tag{95}$$

$$\beta_1^s \approx -\left(s + \frac{1}{2}\right) \sum_{j=1}^{N_\Theta} w_j b_1(\arccos\mu_j) d_{02}^s(\arccos\mu_j), \tag{96}$$

$$\beta_2^s \approx -\left(s + \frac{1}{2}\right) \sum_{j=1}^{N_\Theta} w_j b_2(\arccos\mu_j) d_{02}^s(\arccos\mu_j), \tag{97}$$

where μ_j and w_j are the division points and weights of a Gaussian quadrature formula on the interval $[-1, +1]$. De Rooij and van der Stap [58] showed that a simple *a priori* estimate for the number of quadrature division points in Eqs. (92)–(97) is

$$N_\Theta = 2n_{\max}(|x_{1,\max}|) - 1, \tag{98}$$

where $x_{1,\max} = k_1 R_{\max}$.

To compute the Wigner d-functions entering Eqs. (92)–(97), we use the following upward recursion (see Appendix F of Ref. [56]):

$$\begin{aligned} d_{pq}^{s+1}(\Theta) = {} & \frac{1}{s\sqrt{(s+1)^2 - p^2}\sqrt{(s+1)^2 - q^2}} \\ & \times \{(2s+1)[s(s+1)\cos\Theta - pq] d_{pq}^s(\Theta) \\ & - (s+1)\sqrt{s^2 - p^2}\sqrt{s^2 - q^2} d_{pq}^{s-1}(\Theta)\}, \end{aligned} \tag{99}$$

where $s \geq s_{\min}$ and

$$s_{\min} = \max(|p|, |q|). \tag{100}$$

Note that in general, $d_{pq}^s(\Theta) \equiv 0$ for $s < s_{\min}$. The initial values for the recurrence relation (99) are given by

$$d_{pq}^{s_{\min}-1}(\Theta) = 0 \tag{101}$$

and

$$\begin{aligned} d_{pq}^{s_{\min}}(\Theta) = {} & \xi_{pq} 2^{-s_{\min}} \left[\frac{(2s_{\min})!}{(|p-q|)!(|p+q|)!}\right]^{1/2} \\ & \times (1 - \cos\Theta)^{|p-q|/2} (1 + \cos\Theta)^{|p+q|/2}, \end{aligned} \tag{102}$$

where

$$\xi_{pq} = \begin{cases} 1 & \text{for } q \geq p, \\ (-1)^{p-q} & \text{for } q < p. \end{cases} \tag{103}$$

11.4. Analytical size distribution functions

It is often convenient to approximate naturally occurring and artificial size distributions using simple analytical distribution functions. Our computer program allows the user to choose from the following set of six options:

- the modified gamma distribution

$$n(R) = \text{constant} \times R^{\alpha} \exp\left(-\frac{\alpha R^{\gamma}}{\gamma r_c^{\gamma}}\right); \tag{104}$$

- the log normal distribution

$$n(R) = \text{constant} \times R^{-1} \exp\left[-\frac{(\ln R - \ln r_g)^2}{2\ln^2 \sigma_g}\right]; \tag{105}$$

- the power law distribution

$$n(R) = \begin{cases} \text{constant} \times R^{-3}, & r_1 \leq R \leq r_2, \\ 0, & \text{otherwise}; \end{cases} \tag{106}$$

- the gamma distribution

$$n(R) = \text{constant} \times R^{(1-3b)/b} \exp\left(-\frac{R}{ab}\right), \quad b \in (0, 0.5); \tag{107}$$

- the modified power law distribution

$$n(R) = \begin{cases} \text{constant}, & 0 \leq R \leq r_1, \\ \text{constant} \times (R/r_1)^{\alpha}, & r_1 \leq R \leq r_2, \\ 0, & r_2 < R; \end{cases} \tag{108}$$

- the modified bimodal log normal distribution

$$n(R) = \text{constant} \times R^{-4} \left\{ \exp\left[-\frac{(\ln R - \ln r_{g1})^2}{2\ln^2 \sigma_{g1}}\right] + \gamma \exp\left[-\frac{(\ln R - \ln r_{g2})^2}{2\ln^2 \sigma_{g2}}\right] \right\}. \tag{109}$$

The constant for each size distribution is chosen such that the size distribution satisfies the standard normalization (52).

In principle, particle radii in the modified gamma, log normal, gamma, and modified bimodal log normal distributions can extend to infinity. However, actual computer calculations necessitate choosing a finite $R_{\max}$. As explained in Ref. [29], there are two alternative practical interpretations of a truncated size distribution. The first one is based on increasing $R_{\max}$ iteratively until the far-field optical characteristics of the size distribution converge within a prescribed numerical accuracy. Then the converged truncated size distribution is numerically indistinguishable from the distribution with $R_{\max} = \infty$. The second interpretation assumes that the truncated distribution with a prescribed $R_{\max}$ is a specific size distribution with optical characteristics that can be distinctly different from those of the distribution with $R_{\max} = \infty$. Of course, similar considerations apply to the minimal radius $R_{\min}$, whose implicit value for the modified gamma, log normal, gamma, and modified bimodal log normal distributions is zero, but in practice can be any number smaller than $R_{\max}$.

Two widely used characteristics of a size distribution are the effective radius r_{eff} and effective variance v_{eff}, defined by [62]

$$r_{\text{eff}} = \frac{1}{\langle G \rangle_R} \int_{R_{\min}}^{R_{\max}} \mathrm{d}R\, n(R) R \pi R^2 \tag{110}$$

and

$$v_{\text{eff}} = \frac{1}{\langle G \rangle_R r_{\text{eff}}^2} \int_{R_{\min}}^{R_{\max}} \mathrm{d}R\, n(R) (R - r_{\text{eff}})^2 \pi R^2, \tag{111}$$

where

$$\langle G \rangle_R = \int_{R_{\min}}^{R_{\max}} \mathrm{d}R\, n(R) \pi R^2 \tag{112}$$

is the average area of the geometric projection per particle. By definition, r_{eff} is the projected-area-weighted mean radius, whereas the dimensionless effective variance can serve as a relative measure of the width of the size distribution. All three characteristics in our computer program are calculated by means of the numerical integration over the selected size distribution.

12. Input parameters of the far-field FORTRAN program

- NDISTR, AA, BB, and GAM

The parameter NDISTR specifies the type of the particle size distribution. For the modified gamma distribution (104), NDISTR = 1, AA = α, BB = r_c, and GAM = γ. For the log normal distribution (105), NDISTR = 2, AA = r_g, BB = $\ln^2 \sigma_g$, and GAM is ignored. For the power law distribution (106), NDISTR = 3, AA = r_{eff}, BB = v_{eff}, and GAM is ignored. In this case the parameters R1 = r_1 and R2 = r_2 (see below) are calculated from Eqs. (106) and (110)–(112) for given AA and BB. For the gamma distribution (107), NDISTR = 4, AA = a, BB = b, and GAM is ignored. For the modified power law distribution (108), NDISTR = 5 and BB = α, while AA and GAM are ignored. Finally, for the modified bimodal log normal distribution (109), NDISTR = 6, AA1 = r_{g1}, BB1 = $\ln^2 \sigma_{g1}$, AA2 = r_{g2}, BB2 = $\ln^2 \sigma_{g2}$, and GAM = γ.

- R1 and R2

R1 = $R_{\min}$ and R2 = $R_{\max}$ are, respectively, the minimal and maximal radii in the size distribution for NDISTR = 1–4 and 6. R1 and R2 are calculated automatically for the power law distribution NDISTR = 3 with given r_{eff} and v_{eff}, but they must be specified explicitly for the other distributions. For the modified power law distribution NDISTR = 5, $R_{\min} = 0$, R1 = r_1, and R2 = $r_2 = R_{\max}$.

- LAM

LAM = λ is the wavelength of light in a vacuum.

- CM1 and CM2

CM1 = m_1 and CM2 = m_2 are the complex-valued refractive indices of the host medium and the particle material, respectively. Note that the real and imaginary parts of either refractive index must be non-negative.

- N, NP, and NK

N is the number of equal integration subintervals on the interval [R1, R2] of particle radii. NP is the number of equal integration subintervals on the interval [0, R1] for the modified power law distribution. NK is the number of Gaussian division points on each of the integration subintervals. In other words, N_R = N*NK for NDISTR = 1, 2, 3, 4, 6 and N_R = (N + NP)*NK for NDISTR = 5 in Eqs. (89)–(91).

- NPNA

NPNA is the number of scattering angles at which the normalized scattering matrix (57) is computed. This parameter appears in the PARAMETER statement of the subroutine MATR. The corresponding equidistant scattering angles are given by 180*(I-1)/(NPNA-1) (in degrees), where I numbers the angles. This way of choosing scattering angles can be changed in the subroutine MATR by properly modifying the following lines,

```
N = NPNA
DN = 1D0/DFLOAT(N-1)
```

Table 1
Lorenz–Mie coefficients for Model 1.

n	Re(a_n)	Im(a_n)	Re(b_n)	Im(b_n)
1	0.82786371508743	1.33534702075402	1.40812530318676	0.91474090929954
2	1.42321284483244	0.89127205758731	1.08536531368599	1.20339892215413
3	1.42839459311666	0.87720955358486	1.44609136191343	0.85212694485995
4	1.48435476732684	0.77958526428517	1.65551481250817	0.33539832828945
5	1.60070723150267	−0.22702223626967	1.52109886284329	0.70358935351513
6	1.56230702398572	−0.19914326308055	1.07220921555933	−0.81138512187642
7	1.05356613627414	−0.82013446263817	1.18495350612102	−0.73090304374394
8	0.24879419794541	−0.80037287125636	1.02779612510776	−0.83054387996651
9	−0.12304602444411	−0.14829864230950	−0.09005676783921	0.24630689497581
10	−0.07431723501014	0.28299838641514	−0.04440119340674	0.35883086084932
11	0.27004855985195	0.52830689844492	−0.06364230518866	0.30906391115121
12	0.08166601279635	−0.05469017341575	0.18484082066280	−0.07999366952087
13	0.00974393851164	−0.00725925954865	0.00852881113269	−0.00635976230946
14	0.00139549746752	−0.00085967136799	0.00088184312149	−0.00053112276684
15	0.00018500786241	−0.00008739893067	0.00009269345691	−0.00004181868495
16	0.00002157563095	−0.00000729530239	0.00000891637996	−0.00000279947661
17	0.00000219416116	−0.00000046891364	0.00000076631827	−0.00000014426947
18	0.00000019502761	−0.00000001876110	0.00000005857045	−0.00000000409228
19	0.00000001523117	0.00000000026799	0.00000000398595	0.00000000017899
20	0.00000000105124	0.00000000013737	0.00000000024229	0.00000000003861
21	0.00000000006447	0.00000000001586	0.00000000001320	0.00000000000365
22	0.00000000000353	0.00000000000130	0.00000000000065	0.00000000000026
23	0.00000000000017	0.00000000000009	0.00000000000003	0.00000000000002
24	0.00000000000001	0.00000000000000	0.00000000000000	0.00000000000000

Table 2
Expansion coefficients for Model 2.

s	α_1^s	α_2^s	α_3^s	α_4^s	β_1^s	β_2^s
0	1.0000000	0.0000000	0.0000000	0.8730092	0.0000000	0.0000000
1	2.1374647	0.0000000	0.0000000	2.2880167	0.0000000	0.0000000
2	2.8715833	4.0519444	3.6827289	2.6789587	−0.0761449	0.0380111
3	2.5859159	3.2551090	3.4211813	2.7998748	−0.0687069	−0.0849845
4	2.5448663	3.0650238	2.7702240	2.3491758	−0.1442854	−0.0226902
5	2.0433878	2.2898120	2.4356330	2.2186802	−0.0114772	−0.1799044
6	1.8992339	2.1660811	1.9691485	1.7683300	−0.1094562	−0.0447891
7	1.5730058	1.6458867	1.7280591	1.6870964	0.0243306	−0.1890342
8	1.4403718	1.6146442	1.4916094	1.3652469	−0.0945483	−0.0520282
9	1.2446486	1.2543266	1.2927717	1.3147800	0.0264452	−0.1648505
10	1.1185930	1.2511389	1.1721001	1.0766347	−0.0884296	−0.0601028
11	0.9790658	0.9678685	0.9855668	1.0262673	0.0182229	−0.1309349
12	0.8640150	0.9684714	0.9102400	0.8358930	−0.0827662	−0.0690114
13	0.7402865	0.7253654	0.7373613	0.7783439	0.0095698	−0.0985497
14	0.6419396	0.7229363	0.6725003	0.6162329	−0.0750731	−0.0771134
15	0.5160697	0.5045151	0.5172785	0.5504410	0.0038371	−0.0726803
16	0.4344943	0.4946537	0.4487588	0.4085282	−0.0627630	−0.0832048
17	0.3043668	0.2985595	0.3115572	0.3341546	0.0040266	−0.0555717
18	0.2375074	0.2789122	0.2401043	0.2141354	−0.0413860	−0.0826884
19	0.1185200	0.1172591	0.1265842	0.1400475	0.0121003	−0.0423033
20	0.0837027	0.1063102	0.0723201	0.0596253	−0.0071537	−0.0583147
21	0.0166846	0.0139459	0.0208200	0.0297990	0.0173779	−0.0031417
22	0.0279442	0.0360554	0.0162556	0.0132621	−0.0042381	−0.0182995
23	0.0052215	0.0040493	0.0102754	0.0149044	−0.0007596	0.0041411
24	0.0176142	0.0212466	0.0079960	0.0072768	−0.0055724	−0.0133039
25	0.0027647	0.0028505	0.0040336	0.0052358	0.0003507	−0.0003319
26	0.0055874	0.0066029	0.0012723	0.0010960	−0.0006502	−0.0030844
27	−0.0000270	−0.0000211	0.0007368	0.0009580	−0.0003987	0.0010159
28	0.0011807	0.0013483	−0.0000152	−0.0000074	−0.0008173	−0.0007105
29	0.0000306	0.0000325	0.0000480	0.0000446	0.0000593	−0.0000544
30	0.0000120	0.0000132	0.0000115	0.0000106	0.0000061	−0.0000092
31	0.0000023	0.0000026	0.0000022	0.0000020	0.0000010	−0.0000014
32	0.0000004	0.0000004	0.0000004	0.0000003	0.0000002	−0.0000002
33	0.0000001	0.0000001	0.0000001	0.0000001	0.0000000	−0.0000000

```
DA=DACOS(-1D0)*DN
DB=180D0*DN
TB=-DB
TAA=-DA
DO 500 I1=1,N
   TAA=TAA+DA
   TB=TB+DB
```

and leaving the rest of the subroutine intact. As explained above, this flexibility is provided by the fact that once the expansion coefficients α_p^s ($p=1, 2, 3, 4$) and β_p^s ($p=1, 2$) have been computed by the subroutine SPHER, the scattering matrix can be computed readily for any set of scattering angles using Eqs. (62)–(67).

- DDELT

DDELT is the desired absolute numerical accuracy of the computation of the elements of the normalized scattering matrix.

13. Output information

- R1 and R2

For the power law size distribution (106) corresponding to NDISTR = 3, R1 = r_1 and R2 = r_2 are the minimal and maximal radii, respectively, calculated for the input values of $r_{\rm eff}$ and $v_{\rm eff}$.

- REFF and VEFF

REFF = $r_{\rm eff}$ and VEFF = $v_{\rm eff}$ are the effective radius and effective variance of the size distribution, respectively.

- CEXT and CSCA

CEXT = $\langle C_{\rm ext}\rangle_R$ and CSCA = $\langle C_{\rm sca}^{\rm eff}\rangle_R$ are the ensemble-averaged extinction and effective scattering cross sections per particle, respectively.

- < G >

< G > = $\langle G\rangle_R$ is the average projected area per particle defined by Eq. (112).

- < V >

< V > = $\langle V\rangle_R$ is the average volume per particle defined by

$$\langle V\rangle_R = \frac{4}{3}\int_{R_{\rm min}}^{R_{\rm max}} {\rm d}R\, n(R)\pi R^3. \tag{113}$$

- < R >

< R > = $\langle R\rangle_R$ is the average particle radius defined by

$$\langle R\rangle_R = \int_{R_{\rm min}}^{R_{\rm max}} {\rm d}R\, n(R) R. \tag{114}$$

- Rvw

Rvw = $\langle R_{\rm vw}\rangle_R$ is the volume-weighted average radius defined by

$$\langle R_{\rm vw}\rangle_R = \frac{4}{3\langle V\rangle_R}\int_{R_{\rm min}}^{R_{\rm max}} {\rm d}R\, n(R) R\pi R^3. \tag{115}$$

- SMAX

SMAX = $s_{\rm max}$ is the number of numerically significant expansion coefficients in the series (62)–(67).

- ALPHA1, ..., BETA2

ALPHA1(S) = α_1^s, ALPHA2(S) = α_2^s, ALPHA3(S) = α_3^s, ALPHA4(S) = α_4^s, BETA1(S) = β_1^s, and BETA2(S) = β_2^s are the numerically significant expansion coefficients appearing in Eqs. (62)–(67).

- F11, F33, F12, and F34

F11 = a_1, F33 = a_3, F12 = b_1, and F34 = b_2 are the independent non-zero elements of the normalized Lorenz–Mie scattering matrix (57).

14. Additional comments

It is important to remember that all input parameters having the dimension of length (i.e., r_c, r_g, $r_{\rm eff}$, a, $R_{\rm min}$, $R_{\rm max}$, r_1, r_2, r_{g1}, r_{g2}, and λ) must be specified using the same unit. If these parameters are specified, for example, in micrometers then the output parameters having the dimension of length, area, and volume are given in micrometers, square micrometers, and cubical micrometers, respectively. Consistent with the above discussion, for given size distribution parameters, the parameters N, NP, and/or NK should be increased until converged values are obtained for the extinction and effective scattering cross sections and, especially, the expansion coefficients and the elements of the normalized scattering matrix.

To calculate the scattering characteristics of a monodisperse particle having a radius R, one may use the following options:

```
AA=R
BB=1D-1
NDISTR=4
NK=1
N=1
R1=AA*0.9999999 D0
R2=AA*1.0000001 D0
```

Table 3
Elements of the normalized scattering matrix for Model 2.

Θ (deg)	a_1	a_3	b_1	b_2
0	25.456054	25.456054	0.000000	0.000000
5	22.399261	22.396203	0.060274	0.201144
10	15.779327	15.749295	0.164191	0.487096
15	10.015274	9.947327	0.199128	0.477666
20	6.782489	6.706575	0.158998	0.301982
25	5.054381	4.986203	0.118555	0.208989
30	3.726730	3.658337	0.127304	0.179055
35	2.647274	2.577038	0.149453	0.118842
40	1.929728	1.860128	0.137328	0.054455
45	1.445258	1.376979	0.114033	0.032043
50	1.053837	0.984774	0.108489	0.022028
55	0.769688	0.698467	0.098182	−0.004620
60	0.588748	0.518414	0.073019	−0.020265
65	0.451426	0.381182	0.057267	−0.016630
70	0.344844	0.271144	0.049788	−0.022028
75	0.275779	0.201231	0.033964	−0.030722
80	0.225879	0.152260	0.021187	−0.026080
85	0.185534	0.109331	0.017597	−0.023425
90	0.157508	0.079493	0.011253	−0.026852
95	0.137496	0.060310	0.004902	−0.024740
100	0.121882	0.043423	0.004043	−0.021660
105	0.110854	0.030291	0.004184	−0.022592
110	0.103655	0.022009	0.004175	−0.023809
115	0.099338	0.015470	0.005777	−0.024616
120	0.098229	0.009980	0.009795	−0.026943
125	0.101140	0.005558	0.015832	−0.032475
130	0.108582	0.000647	0.022944	−0.040988
135	0.122316	−0.004952	0.031869	−0.052152
140	0.146394	−0.012032	0.046349	−0.070044
145	0.184628	−0.027396	0.069120	−0.095548
150	0.242246	−0.057445	0.093821	−0.127550
155	0.338232	−0.104198	0.121226	−0.181883
160	0.458863	−0.177361	0.176710	−0.232992
165	0.538532	−0.307051	0.248499	−0.183122
170	0.621883	−0.529260	0.233438	−0.052542
175	0.803057	−0.794203	0.092972	0.006703
180	0.921238	−0.921238	0.000000	0.000000

15. Benchmark numerical results

In this section we illustrate the performance of our computer program and provide accurate numerical results useful for testing purposes. Table 1 lists the numerically significant Lorenz–Mie coefficients a_n and b_n computed for Model 1 represented by a spherical particle with radius R such that $2\pi R/\lambda = 10$. It is further assumed that $m_1 = 1 + {\rm i}0.05$ and $m_2 = 1.53$. Note that the numbers in Table 1 have been computed using both the algorithm described above and an independently written program described in Ref. [11] and based on a different analytical representation of the Lorenz–Mie coefficients. The perfect agreement between these

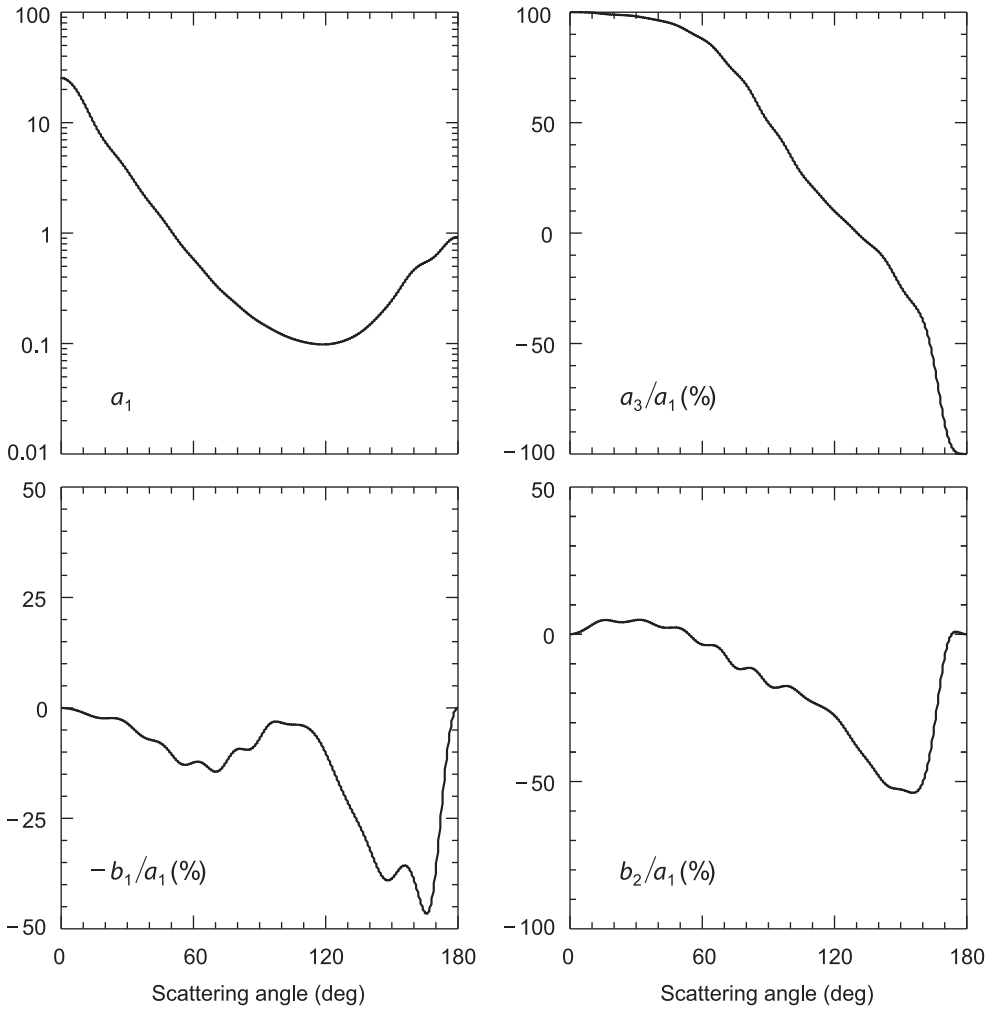

Fig. 4. Elements of the normalized scattering matrix for Model 2.

two sets of results makes the numbers given in Table 1 a well-established benchmark.

Tables 2 and 3 list the expansion coefficients and the elements of the normalized scattering matrix for Model 2 represented by the power law size distribution (106) with $r_{\rm eff}=0.6$ μm and $v_{\rm eff}=0.2$. The vacuum wavelength is $\lambda=0.63$ μm and the refractive indices of the host medium and the particle material are $m_1=1+{\rm i}0.05$ and $m_2=1.53$. The elements of the normalized scattering matrix are also visualized in Fig. 4. Other output parameters are as follows: $\langle C_{\rm ext}\rangle_R=2.07444\ \mu{\rm m}^2$, $\langle C_{\rm sca}^{\rm eff}\rangle=2.99809\ \mu{\rm m}^2$, $r_1=0.245830$ μm, $r_2=1.19417$ μm, $\langle G\rangle_R=0.626712\ \mu{\rm m}^2$, $\langle V\rangle_R=0.501369\ \mu{\rm m}^3$, $\langle R_{\rm vw}\rangle_R=0.720000$ μm, and $\langle R\rangle_R=0.407726$ μm.

It is seen from Table 3 that the elements of the normalized scattering matrix satisfy perfectly the general Lorenz–Mie relations

$$a_3(0)=a_1(0), \tag{116}$$

$$a_3(180^\circ)=-a_1(180^\circ), \tag{117}$$

and

$$b_1(0)=b_2(0)=b_1(180^\circ)=b_2(180^\circ)=0. \tag{118}$$

The coefficient α_1^0 in Table 2 satisfies the identity (74). Furthermore, Table 2 demonstrates the canonical behavior of the expansion coefficients with increasing s: on average, they first grow in absolute value and then decay to values below a reasonable numerical threshold. The fact that the effective scattering cross section exceeds the extinction cross section serves as a vivid demonstration of the intrinsic failure of the notion of the scattering and absorption cross sections in the case of an absorbing host medium.

A natural verification of the above-described computer program is to run it assuming that $m''_1=0$ and compare the results with those obtained with the thoroughly tested conventional far-field program described in Section 5.10 of Ref. [29] and also available at https://www.giss.nasa.gov/staff/mmishchenko/Lorenz-Mie.html. Such comparisons have revealed perfect numerical agreement within the expected accuracy of either program.

Acknowledgments

We thank Guanglin Tang and Nadia Zakharova for help with computations and Fig. 4 and three anonymous reviewers for positive comments and constructive suggestions. This research was funded by the NASA Remote Sensing Theory Program managed by Lucia Tsaoussi and by the NASA Radiation Science Program managed by Hal Maring.

References

[1] Mundy WC, Roux JA, Smith AM. Mie scattering by spheres in an absorbing medium. J Opt Soc Am 1974;64:1593–7.
[2] Chýlek P. Light scattering by small particles in an absorbing medium. J Opt Soc Am 1977;67:561–3.

[3] Bohren CF, Gilra DP. Extinction by a spherical particle in an absorbing medium. J Colloid Interface Sci 1979;72:215–21.
[4] Kamiuto K. Near-field scattering by a large spherical particle embedded in a nonabsorbing medium. J Opt Soc Am 1983;73:1819–22.
[5] Bruscaglioni P, Ismaelli A, Zaccanti G. A note on the definition of scattering cross sections and phase functions for spheres immersed in an absorbing medium. Waves Random Media 1993;3:147–56.
[6] Quinten M, Rostalski J. Lorenz–Mie theory for spheres immersed in an absorbing host medium. Part Part Syst Charact 1996;13:89–96.
[7] Lebedev AN, Gratz M, Kreibig U, Stenzel O. Optical extinction by spherical particles in an absorbing medium: application to composite absorbing films. Eur Phys J D 1999;6:365–73.
[8] Sudiarta W, Chylek P. Mie-scattering formalism for spherical particles embedded in an absorbing medium. J Opt Soc Am A 2001;18:1275–8.
[9] Sudiarta W, Chylek P. Mie scattering efficiency of a large spherical particle embedded in an absorbing medium. J Quant Spectrosc Radiat Transfer 2001;70:709–14.
[10] Fu Q, Sun W. Mie theory for light scattering by a spherical particle in an absorbing medium. Appl Opt 2001;40:1354–61.
[11] Yang P, Gao B-C, Wiscombe WJ, Mishchenko MI, Platnick SE, Huang H-L, et al. Inherent and apparent scattering properties of coated or uncoated spheres embedded in an absorbing host medium. Appl Opt 2002;41:2740–59.
[12] Videen G, Sun W. Yet another look at light scattering from particles in absorbing media. Appl Opt 2003;42:6724–7.
[13] Sun W, Loeb NG, Fu Q. Light scattering by a coated sphere immersed in absorbing medium: a comparison between the FDTD and analytic solutions. J Quant Spectrosc Radiat Transfer 2004;83:483–92.
[14] Sun W, Loeb NG, Lin B. Light scattering by an infinite circular cylinder immersed in an absorbing medium. Appl Opt 2005;44:2338–42.
[15] Fu Q, Sun W. Apparent optical properties of spherical particles in absorbing medium. J Quant Spectrosc Radiat Transfer 2006;100:137–42.
[16] Randrianalisoa J, Baillis D, Pilon L. Modeling radiation characteristics of semitransparent media containing bubbles or particles. J Opt Soc Am A 2006;23:1645–56.
[17] Yin J, Pilon L. Efficiency factors and radiation characteristics of spherical scatterers in an absorbing medium. J Opt Soc Am A 2006;23:2784–96.
[18] Borghese F, Denti P, Saija R. Scattering from model nonspherical particles. Theory and applications to environmental physics. Berlin: Springer; 2007.
[19] Durant S, Calvo-Perez O, Vukadinovic N, Greffet J-J. Light scattering by a random distribution of particles embedded in absorbing media: diagrammatic expansion of the extinction coefficient. J Opt Soc Am A 2007;24:2943–52.
[20] Durant S, Calvo-Perez O, Vukadinovic N, Greffet J-J. Light scattering by a random distribution of particles embedded in absorbing media: full-wave Monte Carlo solutions of the extinction coefficient. J Opt Soc Am A 2007;24:2953–62.
[21] Mishchenko MI. Electromagnetic scattering by a fixed finite object embedded in an absorbing medium. Opt Express 2007;15:13188–202.
[22] Mishchenko MI. Multiple scattering by particles embedded in an absorbing medium. 1. Foldy–Lax equations, order-of-scattering expansion, and coherent field. Opt Express 2008;16:2288–301.
[23] Mishchenko MI. Multiple scattering by particles embedded in an absorbing medium. 2. Radiative transfer equation. J Quant Spectrosc Radiat Transfer 2008;109:2386–90.
[24] Dombrovsky LA, Baillis D. Thermal radiation in disperse systems: an engineering approach. New York: Begell House; 2010.
[25] Ceolato R, Riviere N, Berg MJ, Biscans B. Electromagnetic scattering from aggregates embedded in absorbing media. Prog Electromagn Res Symp Proc Taipei 2013:717–21.
[26] Aernouts B, Watté R, van Beers R, Delport F, Merchiers M, de Block J, et al. Flexible tool for simulating the bulk optical properties of polydisperse spherical particles in an absorbing host: experimental validation. Opt Express 2014;22:20223–38.
[27] Van de Hulst HC. Light scattering by small particles. New York: Wiley; 1957.
[28] Bohren CF, Huffman DR. Absorption and scattering of light by small particles. New York: Wiley; 1983.
[29] Mishchenko MI, Travis LD, Lacis AA. Scattering, absorption, and emission of light by small particles, Cambridge, UK: Cambridge University Press; 2002. <https://www.giss.nasa.gov/staff/mmishchenko/books.html>.
[30] Chandrasekhar S. Radiative transfer. Oxford: Oxford University Press; 1950.
[31] Van de Hulst HC. Multiple light scattering. New York: Academic Press; 1980.
[32] Lenoble J, editor. Radiative transfer in scattering and absorbing atmospheres: standard computational procedures. Hampton, VA: A. Deepak Publishing; 1985.
[33] Tsang L, Kong JA, Shin RT. Theory of microwave remote sensing. New York: Wiley; 1985.
[34] Goody RM, Yung YL. Atmospheric radiation, theoretical basis. Oxford: Oxford University Press; 1989.
[35] Liou KN. Radiation and cloud processes in the atmosphere: theory, observation, and modeling. New York: Oxford University Press; 1992.
[36] Lenoble J. Atmospheric radiative transfer. Hampton, VA: A. Deepak Publishing; 1993.
[37] Mobley CD. Light and water: radiative transfer in natural waters. San Diego: Academic Press; 1994.
[38] Yanovitskij EG. Light scattering in inhomogeneous atmospheres. Berlin: Springer; 1997.
[39] Thomas GE, Stamnes K. Radiative transfer in the atmosphere and ocean. Cambridge, UK: Cambridge University Press; 1999.
[40] Liou KN. An introduction to atmospheric radiation. San Diego: Academic Press; 2002.
[41] Hovenier JW, van der Mee C, Domke H. Transfer of polarized light in planetary atmospheres–basic concepts and practical methods. Dordrecht, The Netherlands: Kluwer; 2004.
[42] Kokhanovsky A. Light scattering media optics. Berlin: Springer; 2004.
[43] Marshak A, Davis AB, editors. 3D radiative transfer in cloudy atmospheres. Berlin: Springer; 2005.
[44] Zdunkovski W, Trautmann T, Bott A. Radiation in the atmosphere. Cambridge, UK: Cambridge University Press; 2007.
[45] Dombrovsky LA, Baillis D. Thermal radiation in disperse systems: an engineering approach. Begell House; 2010.
[46] Howell JR, Siegel R, Mengüç MP. Thermal radiation heat transfer. Boca Raton, FL: CRC Press; 2011.
[47] Wendisch M, Yang P. Theory of atmospheric radiative transfer. Weinheim: Wiley-VCH; 2012.
[48] Modest MF. Radiative heat transfer. San Diego: Academic Press; 2013.
[49] Stamnes K, Stamnes JS. Radiative transfer in coupled environmental systems: an introduction to forward and inverse modeling. Weinheim: Wiley-VCH; 2015.
[50] Box MA, Box GP. Physics of radiation and climate. Boca Raton, FL: CRC Press; 2016.
[51] Mishchenko MI. Electromagnetic scattering by particles and particle groups: an introduction. Cambridge, UK: Cambridge University Press; 2014.
[52] Mishchenko MI. Directional radiometry and radiative transfer: the convoluted path from centuries-old phenomenology to physical optics. J Quant Spectrosc Radiat Transfer 2014;146:4–33.
[53] Stratton JA. Electromagnetic theory. New York: McGraw Hill; 1941.
[54] Rothwell EJ, Cloud MJ. Electromagnetics. Boca Raton, FL: CRC Press; 2009.
[55] Mishchenko MI. Measurement of electromagnetic energy flow through a sparse particulate medium: a perspective. J Quant Spectrosc Radiat Transfer 2013;123:122–34.
[56] Mishchenko MI, Travis LD, Lacis AA. Multiple scattering of light by particles: radiative transfer and coherent backscattering, Cambridge, UK: Cambridge University Press; 2006. <https://www.giss.nasa.gov/staff/mmishchenko/books.html>.
[57] Mishchenko MI, Dlugach JM, Yurkin MA, Bi L, Cairns B, Liu L, et al. First-principles modeling of electromagnetic scattering by discrete and discretely heterogeneous random media. Phys Rep 2016;632:1–75.
[58] de Rooij WA, van der Stap CCAH. Expansion of Mie scattering matrices in generalized spherical functions. Astron Astrophys 1984;131:237–48.
[59] de Haan JF, Bosma PB, Hovenier JW. The adding method for multiple scattering calculations of polarized light. Astron Astrophys 1987;183:371–91.
[60] Wiscombe WJ. Improved Mie scattering algorithms. Appl Opt 1980;19:1505–9.
[61] Abramowitz M, Stegun IA. Handbook of mathematical functions. New York: Dover; 1965.
[62] Hansen JE, Travis LD. Light scattering in planetary atmospheres. Space Sci Rev 1974;16:527–610.